Applied Catalysis B: Environmental 100 (2010) 254–263

Contents lists available at ScienceDirect

Applied Catalysis B: Environmental

journal homepage: www.elsevier.com/locate/apcatb

Al_{13}–[X–Mo/WO_n] (X = Al, Co, V, P) composites as catalysts in clean oxidation of aromatic sulfides

Mercedes Muñoz [a], Gustavo Romanelli [a], Irma L. Botto [b], Carmen I. Cabello [a,*,1], Carole Lamonier [c], Mickael Capron [c], Pascale Baranek [c], Pascal Blanchard [c], Edmond Payen [c]

[a] "Centro de Investigación y Desarrollo en Ciencias Aplicadas, Dr. J. J. Ronco", (CINDECA-CONICET La Plata-UNLP), calle 47 N° 257, (1900) La Plata, Argentina
[b] "Centro de Química Inorgánica" (CEQUINOR), Facultad de Ciencias Exactas, UNLP, (1900) La Plata, Argentina
[c] "Unité de Catalyse et de Chimie du Solide" - UCCS UMR CNRS 8181, Université des Sciences et Technologies de Lille Bât. C3, 59655 Villeneuve d'Ascq Cedex, France

ARTICLE INFO

Article history:
Received 3 November 2009
Received in revised form 30 July 2010
Accepted 3 August 2010
Available online 11 August 2010

Keywords:
Inorganic composites
Heteropolyoxometalates
Al_{13}-polycation
^{27}Al NMR
Raman Microprobe
Selective oxidation of aromatics sulfides
Diphenylsulfide
Dibenzothiophene
Sulfone

ABSTRACT

Several phases of general formula Al_{13}–[XMo_6] (X = Al(III), Co(III), Cr(III), V(V) and Al_{13}–P/[$WO_4]_n$) were prepared by combining the $[AlO_4Al_{12}(OH)_{24}(H_2O)_{12}]^{7+}$ (Al_{13}) Keggin-type isopolycation with different iso or heteropolymetalates such as $[(Al/Co/V)Mo_6O_{24}(H_6)]^{x-}$, $[Co_2Mo_{10}O_{38}H_4]^{6-}$, $[H_2W_{12}O_{40}]^{6-}$ and $[PW_9O_{34}]^{9-}$. The characterization was carried out by means of XRD, ^{27}Al NMR, FTIR and Raman Microprobe techniques. The catalytic activity of bulk composites, structurally constituted by an ordered distribution of the condensed metallic species in an Al(III) oxidic matrix, were proved in two aromatic sulfide oxidation reactions: diphenylsulfide (DPS) to diphenylsulfone in presence of H_2O_2 and dibenzothiophene (DBT) to dibenzothiophenone by means of *tert-butyl* hydroperoxide (*t*-BuOOH). Both reactions were carried out in batch at 80 and 75 °C respectively. Results indicated that oxidation activity improved as the electronic density of the sulfur substrate increased, being higher for DPS (over 90%) than for DBT. Composites based on Anderson heteropolymolybdates presented a better performance in both reactions. ^{27}Al MAS NMR spectroscopic properties can be associated to the catalytic behavior. On the other hand, catalysts based on polytungstates did not show activity except for that containing P as heteroatom. Besides, by ^{27}Al NMR and Raman Microprobe, it was verified that these phases kept their structure after reaction showing an interesting possibility of being re-used.

1. Introduction

The oxidation of aromatic sulfides is a practical and interesting method in petrochemical industry particularly in this new century, when strict environmental regulations are continuously legislated in order to limit sulfur content in fuel oils. On the other hand, the selective oxidation of this type of compounds is also interesting in the pharmaceutical field to produce commodity chemicals as sulfoxides and/or sulfones, easily removed by conventional separation operations [1–6].

In the treatment of petroleum derivatives, a great number of studies on oxidative desulfurization (ODS) have been reported. Technological strategies to reduce the sulfur content in fuel oils were proposed as alternative to the current hydrodesulfurization (HDS) process which involves higher temperature and pressure, larger reactor volume as well as the use of more active catalysts, factors that make the method very expensive [1].

During the last decades, very useful catalytic procedures for sulfide oxidations have been developed involving the use of hydrogen peroxide which promotes the oxidation of the organic substrates due to the effective oxygen-content, it is a low cost product, safe for storage and operation and, mainly, it has an environmentally friendly character. In a similar sense, *tert-butyl* hydroperoxide (*t*-BuOOH) has proved to be an appropriate oxidant, allowing the reaction in organic solution, in batch as well as in fixed bed reactors [6–22]. These obvious advantages have encouraged the development of new catalytic strategies for sulfide peroxide oxidation, including the use of a wide range of catalysts particularly based on the presence of metal or semimetal species [13–19]. So, a discrete number of ODS processes has been reported by different catalysts, oxidants and reaction conditions [23–29]. In this context, with the aim to improve the efficiency and environmental conditions of catalytic processes, the conventional systems (usually Al_2O_3 supported-metal-oxides) have been progressively replaced by the use of condensed phases such as heteropolyoxometalates (HPOMs). Some of them with Anderson-type structure (containing

* Corresponding author at: Chemistry, "Centro de Investigación y Desarrollo en Ciencias Aplicadas, Dr. J. J. Ronco", (CINDECA-CONICET La Plata-UNLP), calle 47 N° 257, (1900) La Plata, Buenos Aires, Argentina. Tel.: +54 221 4220288; fax: +54 221 4210711.
E-mail address: ccabello@quimica.unlp.edu.ar (C.I. Cabello).
[1] Investigador CICPBA.

0926-3373/$ – see front matter © 2010 Elsevier B.V. All rights reserved.
doi:10.1016/j.apcatb.2010.08.001

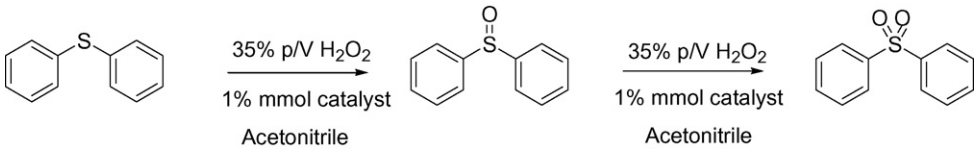

Scheme 1.

Co, Ni or Rh) have recently appeared as interesting hydrotreatment heterogeneous catalysts [30–32] whereas other polyoxometalates (POMs), particularly with Keggin structure, have been applied with success in several ODS processes. The formation of polyoxoperoxo intermediates during the reaction was spectroscopically suggested [3,33–36].

On the other hand, the $[AlO_4Al_{12}(OH)_{24}(H_2O)_{12}][AlMo_6O_{24}]\cdot 29.5H_2O$ phase has been recently reported [37]. This is obtained from the combination of the $[AlO_4Al_{12}(OH)_{24}(H_2O)_{12}]^{7+}$ polycation (hereafter $[Al_{13}]$) and ammonium heptamolybdate [37]. In order to explore new catalytic possibilities for sulfide oxidation that ensure the presence of iso and heteropolymetalates bound to an Al(III) rich matrix, we have recently reported a new form for obtaining the $[Al_{13}]$–$[AlMo_6]$ phase. On this basis, we reported also the preparation, spectroscopic and thermal characterization of two new composites $[Al_{13}]$–$[XMo_6]$ with X = Co and Cr [38,39].

In the present work, the synthesis and catalytic behavior of a series of inorganic composites based on Al_{13}–POMs/HPOMs combination was proposed. The synthesis method includes heteropolyanions derived from Anderson type as $[V^VMo_6O_{24}]^{n-}$ and the dodecamolybdocobaltate $[Co_2Mo_{10}O_{38}H_4]^{6-}$ [32,40,41] as well as the tungstates $[PW_9O_{34}]^{9-}$ and $([H_2W_{12}O_{40}]^{6-}$. Although the structural properties of Al_{13}–$[H_2W_{12}O_{40}]$ have been already reported [42]), the physico-chemical characterization, particularly by ^{27}Al and ^{31}P MAS NMR and Raman Microprobe spectroscopies, can be related to explain the catalytic activity for the diphenylsulfide and dibenzothiophene oxidation reactions which was performed by using 35% p/V hydrogen peroxide and *tert-butyl* hydroperoxide respectively.

2. Experimental

2.1. Synthesis of catalysts

The synthesis of $[AlO_4Al_{12}(OH)_{24}(H_2O)_{12}][XMo_6O_{24}]\cdot 29.5H_2O$ (hereafter $[Al_{13}]$–$[XMo_6]$) was performed by precipitation in aqueous solution and at room temperature according to the following stages:

(a) The polycation $[Al_{13}]$ was prepared from hydrolysis of $AlCl_3.6H_2O$ by NaOH with pH control according to Ho Son method [37].
(b) Several ammoniacal salts of heteropolymolybdates with Anderson structure $[XMo_6O_{24}]^{3-}$ with X = Al, Co and Cr and the $[Co_2Mo_{10}O_{38}H_4]^{6-}$ related phase were obtained as it was previously described [31,32,40,41]. In order to incorporate the V(V) in a structural arrangement Anderson type, an aqueous solution of NH_4VO_3 and HMA was prepared taking into account the stoichiometry corresponding to $[VMo_6O_{24}]^{7-}$ species to be used in an $[Al_{13}]$–$[VMo_6O_{24}]$ composite preparation. In addition, some iso- and heteropolytungstates of sodium or ammonium were used in aqueous solution such as the following polyanions $[H_2W_{12}O_{40}]^{6-}$ and $[PW_9O_{34}]^{9-}$ [42–44].
(c) Preparation of composites by mixture of solutions (a) and (b) at room temperature considering the [Al]/[X+(Mo/W)] = 1.25 ratio.
(d) A polycrystalline precipitate with a different color from that of the heteropolyanion was filtered and dried in air at 80 °C. All solids resulted insoluble in water and organic solvents.

2.2. Characterization techniques

The specific surface area of the synthesized solids was determined from N_2 adsorption at −196 °C on a Micromeritics ASAP 2020 using BET method. Samples were degassed for half an hour at 80 °C before measurement.

The ^{27}Al MAS NMR experiments were carried out on ASX Bruker spectrometers with magnetic field strengths of 9.4 T operating at ^{27}Al Larmor frequencies of 104.3 MHz and using 4 mm MAS probeheads. The ^{27}Al MAS NMR spectra were recorded at spinning rates of 20 kHz using a single pulse excitation sequence with small pulse angle ($\pi/12$) to ensure a quantitative excitation of the central transitions [45] and recycle delay of 4 s. The ^{27}Al triple-quantum MAS (3Q-MAS) spectra [46] were recorded at 9.4 T using the t_1 rotor-synchronized z-filtered pulse sequence [47]. The first two hard-pulse lengths were 2.75 and 1 μs, and the third soft 90° CT pulse length was 21 μs. The recycling delay was 0.5 s and 56 slices were recorded at a spinning speed of 14 kHz. The resonances of the sheared MQ-MAS spectrum were labeled by their normalized ppm coordinates [48] on the MAS and isotropic axes, respectively (δ_{MAS}; δ_{iso}). The ^{27}Al chemical shifts were referenced to 1 M $Al(NO_3)_3$ aqueous solution (pH ∼1).

FTIR spectra were recorded in an interferometer Bruker IFS 66 FTIR (range 400–4000 cm^{-1}) with the technique of KBr pellets. (Not shown in this work.)

Raman Microprobe spectra were performed with a spectrophotometer Raman LabRAM (Infinity microprobe from Jobin-Yvon) equipped with a photodiode array detector. The exciting light source was the 532 nm line of an Nd–YAG laser and the resolution of spectra was 4 cm^{-1}.

The chemical analysis of compounds was carried out in ICP Varian equipment. Likewise, samples were also analyzed by SEM microscopy combined with semiquantitative analysis EDS, with a microscope Philips 505 and analyzer EDAX 9100. These techniques

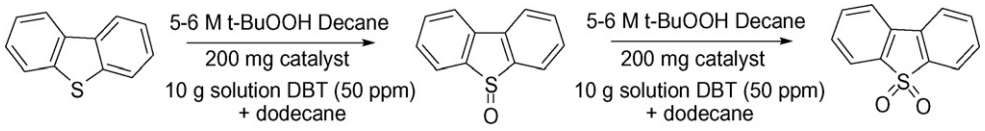

Scheme 2.

were used to control the homogeneity of solids and verify the chemical composition.

2.3. Catalytic test

Two tests of oxidation reactions in batch were used (1) diphenylsulfide to diphenylsulfone using H_2O_2 as oxidizing and (2) dibenzothiophene (DBT) to dibenzothiophene-sulfone ($DBTO_2$) using *t*-BuOOH as oxidizing (Schemes 1 and 2).

2.4. General procedure for oxidation of diphenylsulfide to diphenylsulfone (Scheme 1)

After optimization of the oxidation reaction parameters, the oxidation of diphenylsulfide (DPS) was carried out by heating a solution of 1 mmol of the diphenylsulfide, 0.01 mmol of the catalyst, 1 ml of H_2O_2 35% p/V (~20 mmol) in 5 ml of acetonitrile at 80 °C. The mixture was stirred at 80 °C from 30 min to 2 h. The oxidation reaction was followed by collecting samples from the reaction mixture during reaction at time intervals. GC analyses were performed by a chromatograph VARIAN Star 3400 cx; Column CP SIL 5CB (30 m); FID Detector. Percentages of each compound in the reaction mixture were directly obtained from the corresponding chromatographic peak areas. About 20 μl of the reaction mixture was taken from each sample, which was then diluted in a mixture of water–dichloromethane (2 ml). The dichloromethane layer was dried with anhydrous Na_2SO_4 and filtered. The catalyst was filtered, the solvent was evaporated and the substrate was extracted with dichloromethane (5 ml), washed with water (2× 3 ml) and dried with anhydrous Na_2SO_4. Filtration and evaporation gave rise to the corresponding pure product that was purified by recrystallization to give the pure diphenylsulfone. The diphenylsulfone was identified by ^{1}H NMR, ^{13}C NMR and mass spectrometry.

2.5. General procedure for oxidative desulfurization of dibenzothiophene (Scheme 2)

A solution was prepared with DBT (corresponding to 50 ppm of S) in dodecane with 200 mg of catalyst and 6.5 μl of *tert-butyl* hydroperoxide (5.5 M in decane), corresponding to a molar ratio [*t*-BuOOH]/[S] = 2.3. The reaction was carried out in batch by stirring for 3 h at 75 °C from 10 g of the above-mentioned solution.

The catalyst was separated by filtration and washed with methanol (~5 g) to remove the sulfur retained. The total sulfur contents of feed and product samples were determined using an Antek 9000S Sulfur analyzer (Ultra-Violet fluorescence). Individual Sulfur compound distribution in different samples was determined using a VARIAN CP-3800 gas chromatograph system with autosampler/injector equipped with a 25 m × 0.32 mm × 0.12 μm CP SIL 5CB capillary column (Chrompack) and a Sulfur Chemiluminescence Detector-SCD (Sievers model 355).

3. Results and discussion

Fig. 1 shows the polyhedral representation of the phase whose crystalline structure has been determined by Ho Son et al. [37]. This phase, obtained from the combination of [Al_{13}] polycation with HMA was taken as reference for preparation of new composites by using Anderson phases as starting materials. The composites are structurally constituted by [Al_{13}] polycations and two types of Anderson polyanions (I) and (II) that are joined to the Al-units in two possible ways forming a 3D structure with channels or pores. Polycations [Al_{13}] are formed by twelve $Al(O)_6$ octahedrons distributed in four trimeric planar groups [$Al_3(OH)_6$] that surround a central $Al(O)_4$ tetrahedron forming a ε-Keggin-type structure of Td symmetry [49]. Anderson-type heteropolyanions are formed by a central AlO_6 octahedron joined to six MoO_6 octahedrons in a planar disposition of D_{3d} symmetry [31]. Most composites prepared so far has proved to be isomorphous according to X-ray powder diffraction (not shown here) and Al_{13}–[$AlMo_6$] was the most crystalline species. The remaining phases were poorly crystalline exhibiting, however, the position of the most intense peak of Al_{13}–[$AlMo_6$] [38].

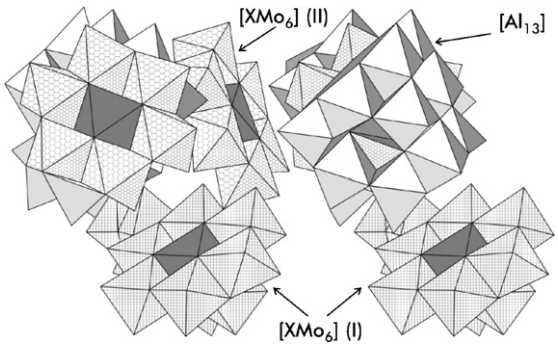

Fig. 1. Polyhedral representation of $[AlO_4Al_{12}(OH)_{24}(H_2O)_{12}][AlMo_6O_{24}]\cdot 29.5H_2O$ according to Ho Son et al. [37]. [Al_{13}] represents the Keggin polycation $[AlO_4Al_{12}(OH)_{24}(H_2O)_{12}]^{7+}$. [$XMo_6$] (I) and (II) represent Anderson heteropolyanions $[XMo_6O_{24}H_6]^{3-}$ that are joined to [Al_{13}] units in two different ways.

The thermal study by TGA–DTA in air atmosphere showed that all species were stable up to 200 °C [38].

For all composites, BET results indicate that the specific area of dried samples is around 35 $m^2\ g^{-1}$.

3.1. Characterization by ^{27}Al and ^{31}P MAS NMR

Fig. 2 presents the ^{27}Al Magic Angle Spinning (MAS) NMR spectra of the three samples Al_{13}–[$AlMo_6$], Al_{13}–[$CoMo_6$] and Al_{13}–[VMo_6]. The spectrum of this species is characterized by the presence of two components [38]. The fit of the first one, located at approximately 61 ppm was easy to determine as the signal corresponding to the Al(t) (tetrahedral coordination) was sharp. The second component around 16.3 ppm was assigned to Al (oct) (octahedral coordination) corresponding to [Al_{12}] polyhedra of the external sphere in the Keggin structure, according to that found by Allouche and Huguenard [50] for the Keggin polycation [Al_{13}] in solution. For the Al_{13}–[$AlMo_6$] phase, a third peak was also

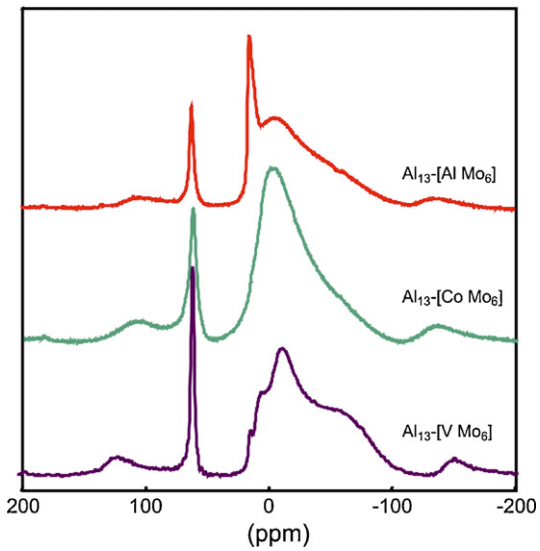

Fig. 2. ^{27}Al NMR (MAS) spectra for Al_{13}–[$AlMo_6$]/–[$CoMo_6$] and –[VMo_6] composites.

Table 1
Assignation of ^{27}Al MAS NMR data for Al_{13}–[XMo_6] with X = Al, Co and V. Isotropical chemical shift in ppm. Al chemical data (e, experimental; t, theoretical) are included.

Phase	δ_{iso} (ppm)	Assign.	Al (%)e-t
Al_{13}–[$AlMo_6$]	61.8	Al(t)	7.5–6.5
	16.3	Al(oct)	79.0–78.5
	14.3	Al(oct)[a]	13.5–15.0
Al_{13}–[$CoMo_6$]	63.0	Al(t)	9.0–7.7
	15.0	Al(oct)	91.0–92.3
Al_{13}–[VMo_6]	60.6	Al(t)	8.7–8.0
	(**#1**) 16.8	Al(oct)[a]	1.9e
	(**#2**) 11.4		
	(**#3**) 11.8[b]	Al(oct)	24.6e
	(**#4**) 7.5[c]		64.8e

(**#1**)–(**#4**): calculated values from fitting of MQ-MAS positions.
[b]MQ and [c]Czjzek model used for fitting: [b](C_Q: 9.5 MHz, η_Q: 0.2); [c](C_Q: 5 MHz, η_Q: 0.6) [51,52].
[a] Position assigned to Al of heteropolyanion [$AlMo_6$].

observed, located at 14.3 ppm and assigned to Al(oct) belonging to central [AlO_6] group of Anderson polyanion [38]. This line was very clear due to the high symmetry of the Al(III) environment in the Anderson structure. Table 1 shows the relative aluminum amount for the tetrahedral and octahedral sites, calculated for the phase from experimental data. Theoretical values are included as reference. These values are in agreement with the ones calculated based on the ideal formula [37].

The spectrum of the Al_{13}–[$CoMo_6$] new phase was composed by two signals at 63 ppm and at 15 ppm attributed to Al(t) (AlO_4) and Al(oct) (AlO_6) of Keggin structure respectively. The slight shift observed with respect to Al_{13}–$AlMo_6$ reference species was produced by the different interaction of $CoMo_6$ with Al Keggin matrix. The relative Al amount obtained with the method was acceptable according to the theoretical values.

In the case of Al_{13}–[VMo_6], the second component was much broader, centered around 0 ppm, and assigned to aluminum in octahedral local environment and obviously, this part of the spectra was an overlap of many resonances. The fit of this part of the spectra was not direct.

In order to fit the different spectral components, the ^{27}Al NMR Multi Quantum (MQ) MAS experiment was performed on the Al_{13}–[VMo_6], which is shown in Fig. 3.

The signal of the Al(t) contribution was very sharp and located at δ_{iso} (isotropic chemical shift) = 60.6 ppm. On the other hand, the part of the spectrum corresponding to the aluminum Al(oct) coordinated was zoomed, as it is presented in Fig. 4. The fit of these 2D experiments was obtained using the DM fit program [51]. Table 1 shows the position of four lines used to get a better fit for the Al(oct) signal: two lower (#**1** and #**2**) and two main (#**3** and #**4**).

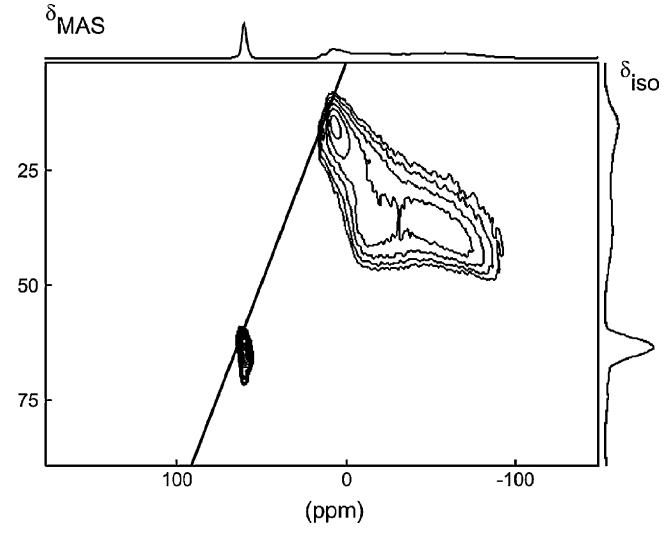

Fig. 3. ^{27}Al NMR Multi Quantum (MQ) MAS experiment for Al_{13}–[VMo_6] composite.

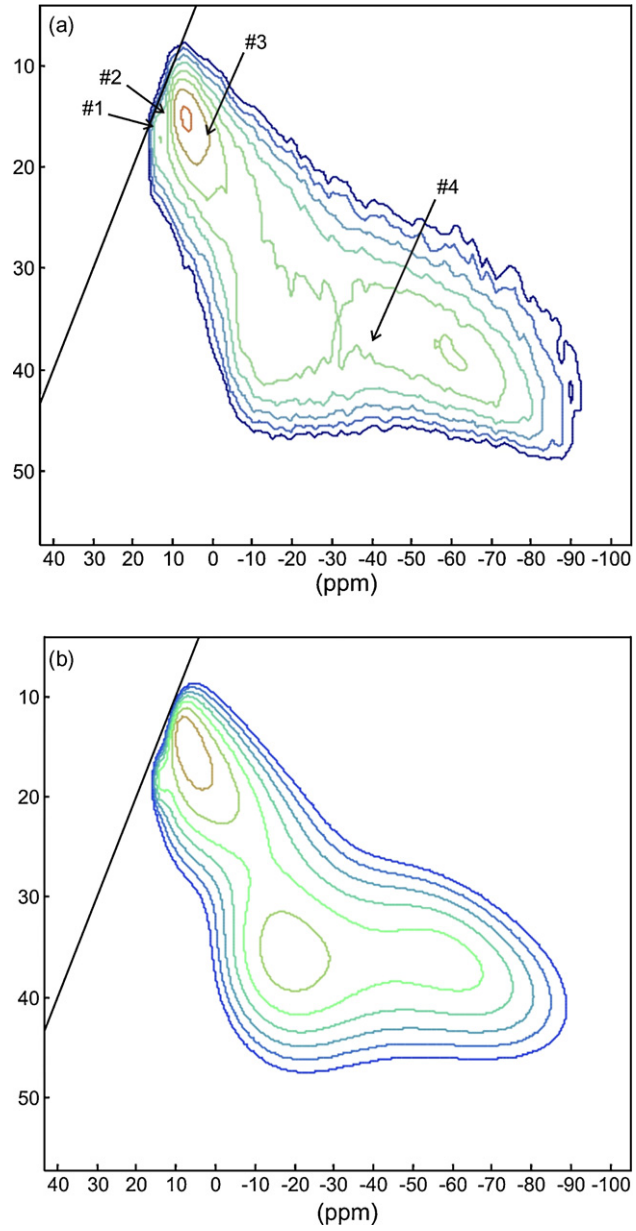

Fig. 4. (a) Experimental and (b) theoretical zoomed parts of the ^{27}Al NMR MQ-MAS spectrum corresponding to Al (oct) for Al_{13}–[VMo_6] composite. References #**1**, #**2**, #**3** and #**4** are indicated in the text.

From the quantitative analysis, the two lower resonances (#**1** and #**2**) represented less than 2% of the total aluminum atoms present in the sample. According to the isotropic chemical shift of these lines, it is possible to associate them to Al(oct) of $[AlMo_6H_6O_{24}]^{3-}$ Anderson species, in accordance with our previous work [38,36,51]. The other two resonances (#**3** and #**4**) represented 89.4% of the total aluminum atoms. Considering only the three main lines located at 60.6 Al(t), and (7.5 and 11.8) Al(oct) ppm, a value of 9:91 for the Al(t)/ Al(oct) ratio was in agreement with the theoretical one for the Al_{13} cation (8:92). Therefore, regarding the aluminum quantification, the isotropic chemical shift and the quadrupolar parameters allowed us to corroborate the presence of Al_{13} structure in Al_{13}–[VMo_6].

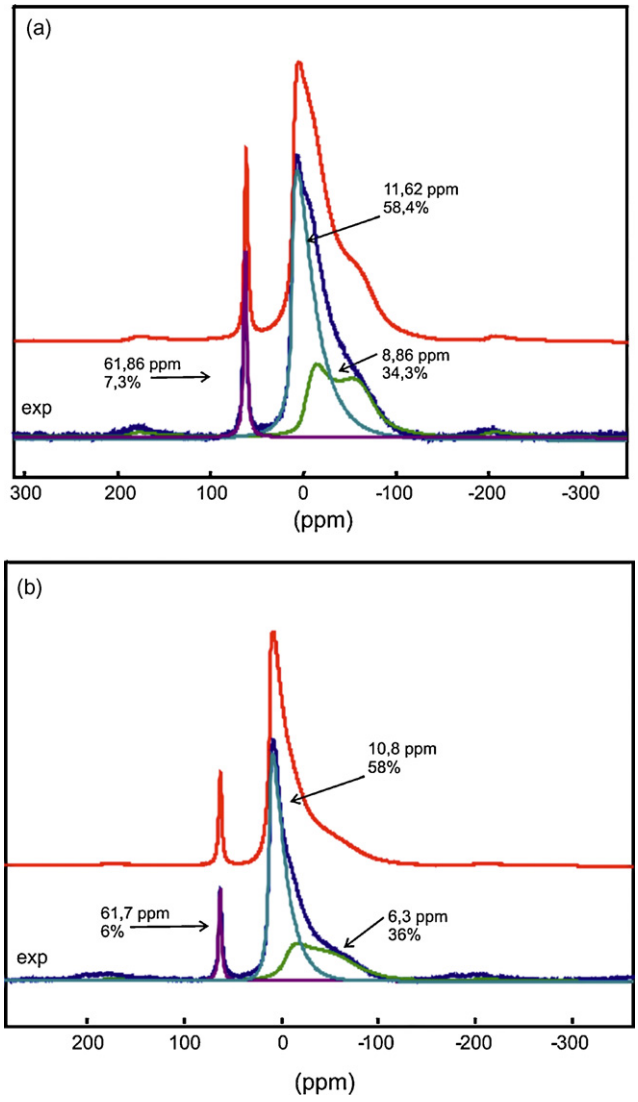

Fig. 5. ^{27}Al NMR (MAS) spectra for (a) Al_{13}–$[PW_9O_{34}]$ and (b) Al_{13}–$[H_2W_{12}O_{40}]$ composites.

Moreover, considering only the Al atoms in octahedral coordination, the distribution between the two lines (#**4** and #**3**) showed that there are two types of aluminum of Keggin polycation which are in a ratio about 9:3. Hence, a remarked decrease of symmetry can be expected.

Fig. 5(a) and (b) shows ^{27}Al MAS spectra of Al_{13}–$[H_2W_{12}O_{40}]$ and Al_{13}–$[PW_9O_{34}]$ composites. The first species prepared from ammonium metatungstate has been recently reported as δ-Al_{13}–$[H_2W_{12}O_{40}]$ using a different synthesis method [42]. The second one was prepared for the first time using $Na_8H[PW_9O_{34}]$ lacunar phosphotungstate [44]. As it was previously mentioned, spectra of these phases were composed by two contributions. One of them was sharp and located at δ_{iso} 61.9 ppm for Al_{13}–$[PW_9O_{34}]$ (7.3% of the total aluminum atoms) and δ_{iso} 61.7 ppm for Al_{13}–$[H_2W_{12}O_{40}]$ (6% of the total aluminum atoms). These isotropic chemical shifts were characteristic of Al(t). The second one consisted of an overlap of two resonances. The shapes were determined with the help of the ^{27}Al MQ-MAS experiment. The Al(oct) signal for the Al_{13}–$[PW_9O_{34}]$ sample (Czjzek model [52]) is located at δ_{iso}: 11.6 ppm (C_Q: 5.5 MHz, η_Q: 0.6) and the fitting by a quadrupolar model gave a signal located at δ_{iso}: 8.9 ppm (C_Q: 9.7 MHz, η_Q: 0). The Al(tet)/Al(oct) ratio (expressed in %Al) was 6/94, in agreement with the ε-Al_{13} structure. For the Al_{13}–$[H_2W_{12}O_{40}]$ sample, the first Al(oct) signal characterized by the Czjzek model was located at δ_{iso}: 10.8 ppm (C_Q: 4.1 MHz, η_Q: 0.6) and the second one fitted by a quadrupolar model was located at δ_{iso}: 6.3 ppm (C_Q: 9.2 MHz, η_Q: 0). Again the Al(tet)/Al(oct) ratio was 7/93. The δ_{iso} and the quadrupolar parameters were in agreement with the ε-Al_{13} structure which was locally disordered because of the counter anion. These parameters were different from the ones corresponding to isomer δ-Al_{13}–$[H_2W_{12}O_{40}]$ whose values were: δ_{iso} 64.7 ppm for Al(t) and a peak near 0 ppm for the Al(oct) [42].

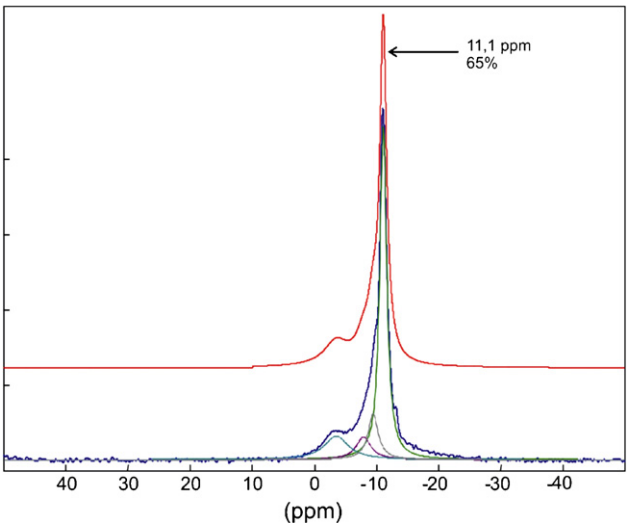

Fig. 6. ^{31}P NMR spectrum for Al_{13}–$[PW_9O_{34}]$ composite.

In order to complement the characterization of species containing Al and P, additional measurements by ^{31}P MAS NMR spectroscopy were performed and shown in Fig. 6. The spectrum is composed, at least, by four overlapping resonances, indicating that the Al_{13}–$[PW_9O_{34}]$ phase was partially decomposed. The ^{31}P peak located at δ_{iso} -11,1 ppm corresponds to approximately 65% of phosphorous atoms present in the solid and it was assigned to -$[PW_9O_{34}]$ entities. The assignment of the other peaks was not performed.

The results for the Al_{13}–$[H_2W_{12}O_{40}]$ solid phase were quite different and showed the presence of polyanion in the Al_{13}–$[H_2W_{12}O_{40}]$.

Summarizing, ^{27}Al MAS NMR is a useful technique to confirm the presence of $[Al_{13}]$ polycation in all studied species although it suggests the presence of the $AlMo_6$ Anderson species in the Al_{13}–$[VMo_6]$ composite.

3.2. Characterization by Raman Microprobe

The assignment of vibrational FTIR as well as Raman composite spectra under study was basically performed as a function of structural units that form the HPOM connected to the matrix $[Al_{13}]$. This is due to the fact that the polycation was only characterized by the stretching band corresponding to the Al–OH bond which appears as a weak shoulder at 1003 cm^{-1} in FTIR [38].

The nature of this mode did not allow its observation by Raman [53]. However, Microprobe Raman, seems to be the most adequate for characterization of principal vibration modes of terminal M-O bonds and M-O-M bridges with M = Mo or W. Fig. 7 shows comparative Raman spectra (from 200 to 1200 cm^{-1}) of two composites: Al_{13}–$[AlMo_6]$ and Al_{13}–$[CoMo_6]$ with their corresponding Anderson-type polyanions: $AlMo_6$ and $CoMo_6$. For ammonium salts, Raman lines characteristic of the ν_s Mo–O_{2t}, symmetric stretching was observed around 945 cm^{-1}. These lines were intense and clear, unlike those corresponding to the ν_{as} Mo–O_{2t} asymmet-

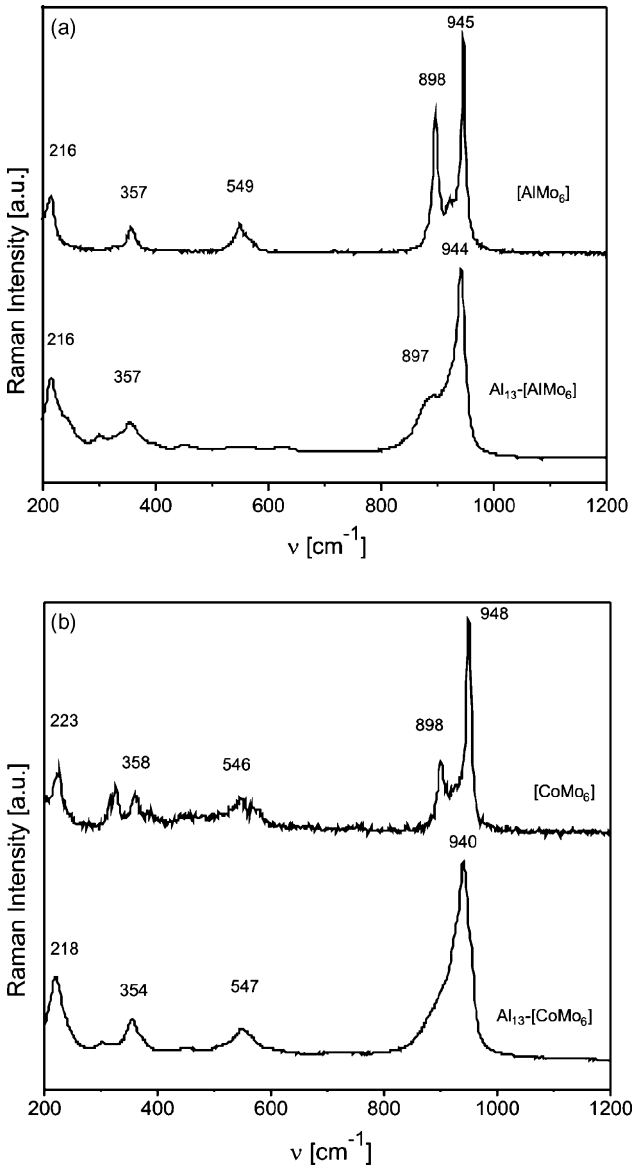

Fig. 7. Comparative Raman Microprobe spectra for (a) Al_{13}–[$AlMo_6$] and (b) Al_{13}–[$CoMo_6$] composites and respective [$AlMo_6$], [$CoMo_6$] Anderson HPOMs.

ric mode located at about 892 cm^{-1} [38]. Lines around 545 cm^{-1} corresponded to the bridge bond characteristic of Mo–O–X bonds. These three types of lines were very sensitive to the heteroatom type, and in general it was observed that the frequency ν_s Mo–O_{2t} increased with the ionic radius of the heteroatom [rAl(III) < rCo(III)]. Comparing these two types of solids, slight frequency shifts were observed and this can be attributed to interaction effects produced by the insertion of the heteropolyanion into the [Al_{13}] polycation matrix [38].

From the analysis of such results, it was possible to prove that the Anderson structure of HPOMs was preserved in the reticular system formed with the [Al_{13}] matrix. Fig. 8 shows the Raman spectrum of the vanadium based composite. This last showed certain similarity with the rest of composites. However, the extra line at 986 cm^{-1} can surely be attributed to a strong bond V=O. This mode appeared at a lower frequency than that observed in V_2O_5 (994 cm^{-1}). Thus, V(V) could be found in the center of a distorted polyhedron derived from an Anderson structure. It is possible to suggest a decreasing of the symmetry. In the hypothetical and extreme case of tetrahedral environment, the V(V)

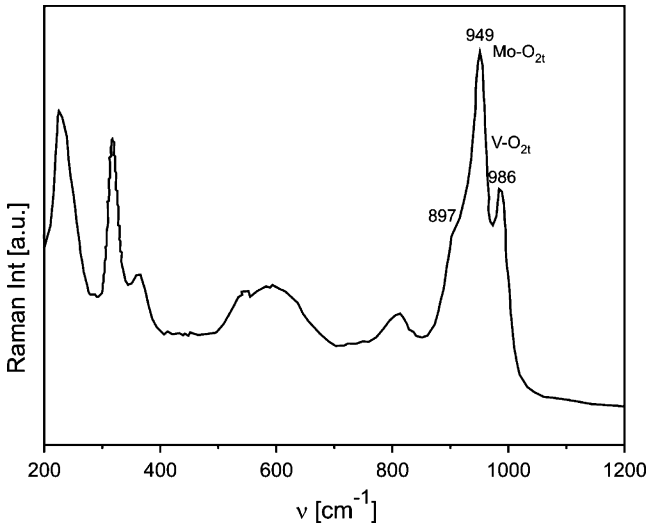

Fig. 8. Raman Microprobe spectrum for Al_{13}–[VMo_6] composite (between 200 and 1200 cm^{-1}).

heteropolymolybdate structure could be constituted by two central VO_4 tetrahedrons as in the heteropolyanion $[V_2Mo_6O_{26}]^{6-}$ whose structure, shown in Fig. 9, was determined crystallographically by Björnberg [54]. On the basis of Raman results and with the aid of Hardcastle's expression [$\nu\,cm^{-1} = 21{,}349 \exp(-1.9176\,d\,Å)$] [55], it is possible to suggest a V–O bond length = 1.61 Å which was similar to that observed for the shorter V–O bonds for tetra and pentacoordinated vanadium (V) compounds. According to our results, it may be possible that [Al_{13}] as countercation could stabilize the Björnberg heteropolyanion instead of the hypothetical phase of formula $[VMo_6O_{24}]^{7-}$.

The composite chemical analysis was determined by ICP technique (Mo % 63.3; Al % 29.4 and V % 7.3 considering only metals). The theoretical values deduced from the formation of Al_{13}–[VMo_6O_{24}] entities were Mo 59%, Al % 36 and V 5% whereas those deduced for Al_{13}–[$V_2Mo_6O_{26}$] were: Mo: 56%, Al 34% and V 10%. In this case and comparing ^{27}Al NMR and Raman results, it is evident that a mixture of composites containing $AlMo_6$ and V_2Mo_6 was formed.

Fig. 10(a) and (b) shows lacunar Na-phosphotungstate and ammonium-metatungstate Raman spectra which were compared with the respective composites: Al_{13}–[PW_9O_{34}] and Al_{13}–[$H_2W_{12}O_{40}$]. The [PW_9O_{34}] structure was collapsed when interacting with Al_{13} matrix confirming also results obtained by ^{31}P MAS NMR. However, the characteristic lines of metatungstate species reveal the conservation of the isopolytungstate-ions, result previously evidenced by NMR spectroscopy.

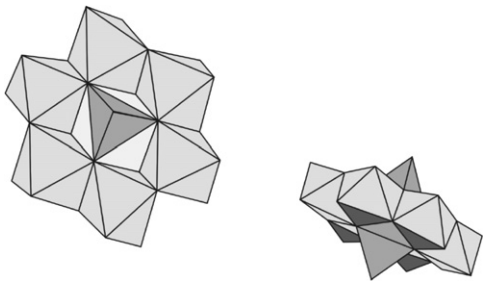

Fig. 9. Polyhedral representation of HPOMs $[V_2Mo_6O_{26}]^{6-}$ structure according to Björnberg [54].

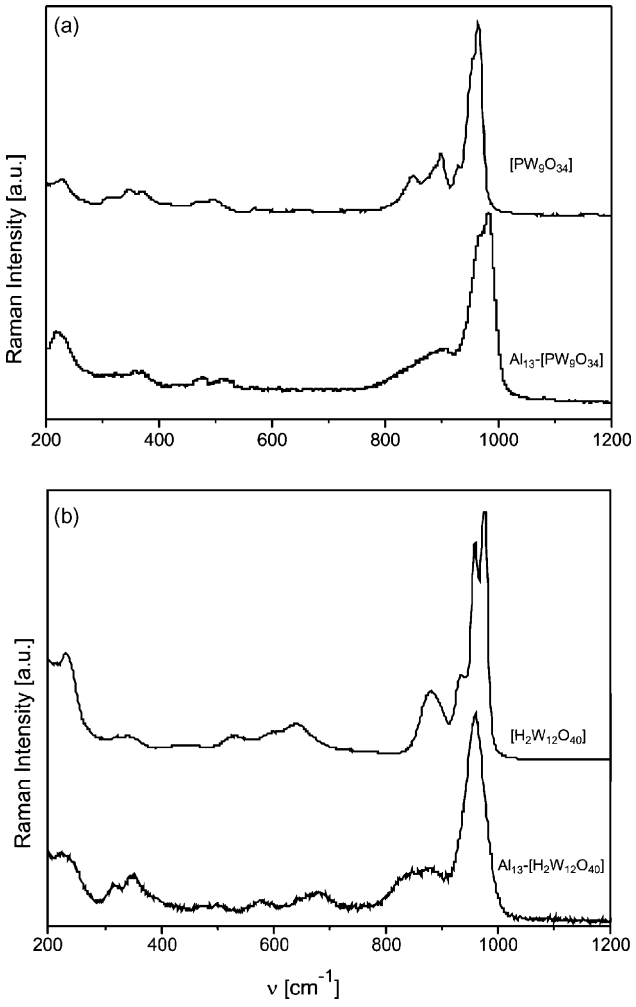

Fig. 10. Comparative Raman Microprobe spectra for ammonium metatungstate and Na lacunar phosphotungstate and their respective composites Al_{13}–$[H_2W_{12}O_{40}]$ and Al_{13}–$[PW_9O_{34}]$.

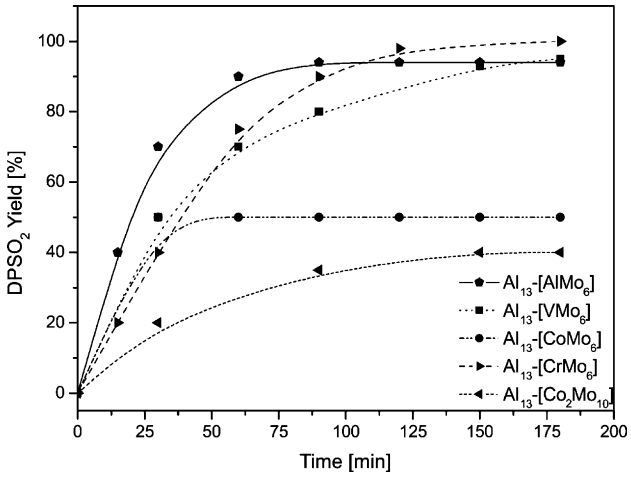

Fig. 11. Relationships between diphenylsulfone yield and time for the studied Anderson-derived composites as catalysts for DPS oxidation by H_2O_2 at 80 °C in acetonitrile.

3.2.1. Catalytic results

Table 2 shows results obtained for all catalysts used in the oxidation reaction of diphenylsulfide to diphenylsulfone, where the conversion of diphenylsulfide was expressed and calculated according to its disappearance. Very low conversion, 50% in 24 h in acetonitrile reflux at 80 °C, was obtained in catalyst absence, but when a composite was added, the reaction time was reduced considerably and the conversion increased to values close to 100% (Table 2). The results obtained show that DPS conversion depends strongly on the nature of the catalysts.

Regarding the Anderson-derived composites, it is observed that: when Al_{13}–$[AlMo_6]$ composite was used (Table 2), a conversion of 100% was observed after 45 min, in reflux of acetonitrile (80 °C). A yield of sulfone was obtained from this catalyst in 70 min with 94% of selectivity and no secondary products were detected. Using Al_{13}–$[CoMo_6]$, a conversion equal to 100% was also easily obtained (30 min) but the selectivity was poor, only 50% in 150 min. Moreover, Al_{13}–$[Co_2Mo_{10}]$ was far less active than the other composites. Only 80% conversion was obtained in 240 min with 40% selectivity.

Very high conversion (100%) and selectivity (93%) were also obtained for the suggested Anderson Al_{13}–$[VMo_6]$ derived species but in order to obtain such performances it was necessary 150 min for running this reaction. This behavior could be compared to that corresponding to Al_{13}–$[CoMo_6]$ phase. Finally, Cr derived showed less activity and a better selectivity to sulfone when the reaction was over. Fig. 11 shows the relationships between diphenylsulfone yield and time for the studied Anderson-derived compounds.

It could be suggested the following activity order for Anderson-derived "composites" as catalysts in diphenylsulfide selective oxidation:

$$Al_{13}\text{–}[AlMo_6] > Al_{13}\text{–}[VMo_6] = Al_{13}\text{–}[CrMo_6] > Al_{13}\text{–}[CoMo_6] > Al_{13}\text{–}[Co_2Mo_{10}].$$

Taking into account this activity order, it was calculated the reaction rate of DPS oxidation, in H_2O_2 in the above-mentioned conditions, using the obtained data for more active catalysts: Al_{13}–$[AlMo_6]$, $[VMo_6]$ and $[CrMo_6]$. In all cases the reaction rate was of 2nd order, but in Fig. 12 it is shown the linear fit for the more active phase Al_{13}–$AlMo_6$. Likewise, Fig. 13 shows a typical profile for the evolution of DPS oxidation reaction, where the sulfoxide and sulfone formation were obtained by consecutive steps (see Scheme 1).

It was possible to correlate this activity sequence with different structural properties, particularly those regarding nuclear magnetic resonance of the materials.

Table 2
Conversion and selectivity data obtained for oxidation of diphenylsulfide.

	Catalyst	Diphenylsulfide conversion (%)	Diphenylsulfoxide selectivity (%)	Diphenylsulfone selectivity (%)	Time[a] (min)
1.	Al_{13}–$[AlMo_6]$	100	6	94	70
2.	Al_{13}–$[VMo_6]$	100	7	93	150
3.	Al_{13}–$[CoMo_6]$	100	50	50	150
4.	Al_{13}–$[CrMo_6]$	90	2	98	120
5.	Al_{13}–$[Co_2Mo_{10}]$	80	60	40	240
6.	Al_{13}–$[PW_9O_{34}]$	100	2	98	80
7.	Al_{13}–$[H_2W_{12}O_{40}]$	100	20	80	120

[a] Time for which the presented selectivity were obtained.

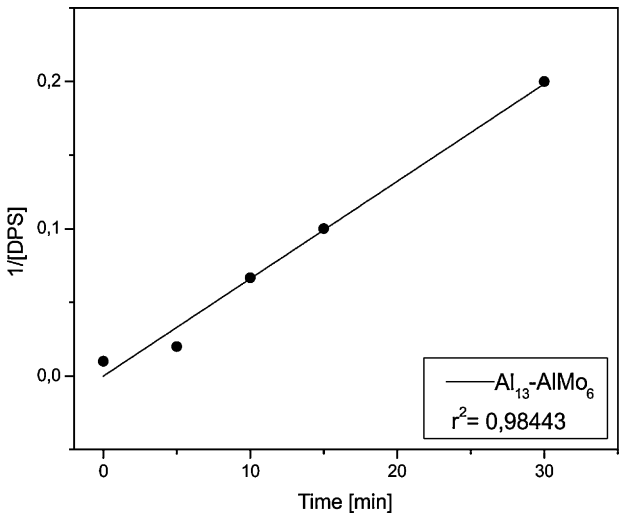

Fig. 12. Plot of the 2° order rate of the oxidation reaction of DPS by H_2O_2 at 80 °C in acetonitrile, catalyzed by Al_{13}–[$AlMo_6$].

In fact, as above mentioned, the different ^{27}Al MAS NMR bands corresponding to tetrahedral Al and octahedral Al depend on the character of the heteroatom from Anderson unit. Thus, it was possible to observe an increase of the band area of Keggin octahedral Al in the "composite" containing Co if compared to values of Al_{13}–[$AlMo_6$] and [VMo_6] phases, Table 1 and Fig. 2. Although the Al_{13}–[VMo_6] spectrum was more complex than the other, this species showed again an increase of area assigned to Al(oct) Keggin whose signal resulted the most sensitive for this species and suggested a lower symmetry for Al (oct) in the Keggin polycation. Then, it was possible to observe the sequence: Al_{13}–[$AlMo_6$](79.0%) < Al_{13}–[VMo_6](89.4%) < Al_{13}–[$CoMo_6$](91.0%) which is opposite to the catalytic activity. The composite Al_{13}–[$AlMo_6$] is in fact a system which explains its good performances. The activity of Al_{13}–[VMo_6] is related to the exact nature of this solid as evidenced by NMR and Raman spectroscopies. It was previously shown that this catalyst contains, in fact, $AlMo_6$ entities, which may be partly responsible for the catalytic performances.

Composites catalytic behaviors are in agreement with results reported in the literature for oxidation reactivity of polyoxometalates containing Mo and V and phosphotungstic acids in general

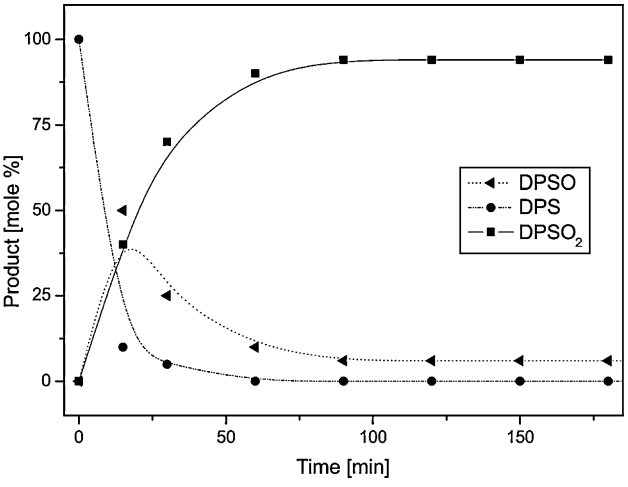

Fig. 13. Time progression of substrate and products concentrations for DPS oxidation by H_2O_2 at 80 °C in acetonitrile catalyzed by Al_{13}–[$AlMo_6$].

Table 3
Oxidative desulfurization activity for composites in dibenzothiophene (DBT) to dibenzothiophene-sulfone ($DBTO_2$).

Catalyst	DBT conversion (%)
Al_{13}–[$CoMo_6$]	22.5
Al_{13}–[VMo_6]	22.2
Al_{13}–[$AlMo_6$]	19.0
Al_{13}–[$CrMo_6$]	4.6
Al_{13}–[Co_2Mo_{10}]	10.0
Al_{13}–[PW_9O_{34}]	19.6
Al_{13}–[$H_2W_{12}O_{40}$]	–

[3]. Particularly, the Mo(W)–Al–O systems appears as the best candidate for oxidation of sulfur-based molecules.

Regarding W species, it was observed that [PW_9O_{34}] derivative was the most active. When Al_{13}–[PW_9O_{34}] is used as a catalyst, the reaction gives rise to the highest conversion and selectivity. A 100% of diphenylsulfide conversion was obtained after 30 min and 98% of sulfone selectivity after 80 min of reaction at 80 °C. Lower selectivity was observed for Al_{13}–[$H_2W_{12}O_{40}$].

In agreement with literature data, species based on heteropolytungstates, catalytic results indicate that those containing P presented better performance than the ones without this element. It has been stated that phosphomolybdic as well as phosphotungstic species are catalytic precursors that produce active polyoxoperoxo complexes during reaction. The good reactivity of catalysts containing [P–W–O] groups compared to other polytungstates containing [W–O] groups is also explained by the formation of peroxocomplexes of "lacunary species". These are, e.g. $PO_4[MO(\mu\text{-}O_2)(O_2)]_4^{3-}$ [33,36] or $PO_4[MO(\mu\text{-}O_2)(O_2)]_2^{3-}$ with M = Mo or W [35]. It is possible that in the studied reaction, the Al_{13}–[PW_9O_{34}] composite may favor the formation of an intermediate "lacunar binuclear peroxo" containing P of the type above mentioned [35,56].

3.3. Oxidation of dibenzothiophene (DBT) to dibenzothiophene-sulfone ($DBTO_2$)

DBT was selected as it is one of the most representative sulfides from those present in gasoil. The reaction was performed at 75 °C for 3 h. Selected conditions corresponded to the classic test where catalysts of the Mo/alumina series are used with *t*-BuOOH as oxidant widely used for desulfurization of heavy petroleum cuts [2].

Table 3 shows results obtained for all catalysts used in the oxidation reaction of dibenzothiophene (DBT) to dibenzothiophene-sulfone ($DBTO_2$). No formation of dibenzothiophene-sulfoxide was observed whatever the catalyst.

The larger conversion to $DBTO_2$ obtained was lower than 25% which seems very low by comparison with the catalytic performances obtained with diphenylsulfide. This can be explained by the lower electronic density on the sulfur atom of DBT compared to diphenylsulfide [57]. It is well know that the divalent sulfur of DPS and DBT can be oxidized by the electrophilic addition reaction of oxygen atoms to the tetravalent and hexavalent sulfur of DPS and DBT (sulfoxide or sulfone, respectively). Hence, the reactivity of oxidation becomes higher for a sulfur atom with a higher electron density. The electron density of sulfur for DPS and DBT are 0.360 and 0.450, respectively (we calculated the charge over the sulfur atom, using a Hyper ChemTM 5.0 Release for windows program) [3].The fact that DBT remained the most difficult to be oxidized can be explained by the much lower electron density of sulfur atom in DBT compared with those in DPS. In addition a complementary steric-hindrance due to the heterocyclic system in DBT could also be considered, when the sulfur in DBT was adsorbed on the surface of the catalytic system. Moreover the oxidant/substrate molar ratios

Table 4
Conversion data of DBT for Al_{13}–[$AlMo_6$]/[Co_2Mo_{10}] composites untreated and calcined at 200 °C.

Catalyst	Conversion of DBT (%)[a]
Al_{13}–[$AlMo_6$]	
Untreated	19.0
Calcined at 200 °C	26.9
Al_{13}–[Co_2Mo_{10}]	
Untreated	10.0
Calcined at 200 °C	28.3

[a] 75 °C for 3 h.

used were not the same for the two tests (H_2O_2/phenylsulfide = 20 and *t*-BuOOH/DBT = 2.3) which may imply different reactivity.

Comparison of catalytic performances of different solids indicated almost a similar order than that previously observed for diphenylsulfide oxidation. Indeed, the [$AlMo_6$] and [VMo_6] species are into the ones that presented the highest activities while the lowest performances were reported for [Co_2Mo_{10}] and [$CrMo_6$] based solids. In addition coinciding with the result found for the oxidation of DPS, the composite Al_{13}–[PW_9O_{34}] was more active than Al_{13}–[$H_2W_{12}O_{40}$]. As reported before, presence of phosphorus in catalysts based on tungstic acids favors formation of "peroxo" intermediate bi or tetranuclear species which facilitates the interaction of peroxo bonds with c–c bonds [35,56]. The behavior of Al_{13}–[$CoMo_6$] is not yet clearly understood since this solid showed the best reactivity in DBT oxidation while it was one of the worse catalysts in ODS of diphenylsulfide. Work is now under progress to explain this result.

Table 4 shows DBT conversion in the ODS reaction catalyzed by Al_{13}–[$AlMo_6$] and Al_{13}–[Co_2Mo_{10}] composites before calcination (untreated catalysts) and after calcination at 200 °C. The conversion increased from 18% to 26.9% for Al_{13}–[$AlMo_6$] and from 10% to 28.3% for Al_{13}–[Co_2Mo_{10}]. These results suggest that the thermal treatment produces a structural transformation not only dehydrating the complex but also improving the availability of active sites on the solid surface. Especially the Co_2Mo_{10}-based one, whose original structure was not planar, could be transformed into an Anderson-type planar structure by thermal effect as it was explained in previous studies [34].

When intending to analyze the chemical composition composites as "supported" phases in an Al(III) oxidic matrix, the total content of Mo + metal X (~35%) is high if compared with those conventional catalysts with around 15% of Mo supported on alumina. Dispersion of these Mo(W) phases on this Al-matrix is good since no bulk oxide such as MoO_3 is observed. Thus we could think that the activity of our solids should be higher than that of classical solids previously presented in the state of art. In the composite, the structure presents a regular order of "clusters" [X/Mo/W/O] anchored to the Al_{13} matrix and the structural disposition intercluster (Al_{13} nets inserted among nets of polyanions) provides planes where only one of the two anionic unities is mostly exposed as it is shown in Fig. 14 according to Ho Son et al. [37]. Therefore, this feature hinders the total availability of active sites especially in the case of phases containing orderly Anderson HPOMs like $AlMo_6$ and $CoMo_6$. From this analysis, it is possible to suggest that the high content of metals (Mo/W + X) would remain partially inhibited by structural effects.

3.4. Characterization of Al_{13}–[$AlMo_6$] and [VMo_6] after catalytic reaction

In order to investigate the re-use of species under study, some composites were separated by filtration, washed with methanol, dried and characterized by Raman Microprobe and XRD. Fig. 15 shows Raman Microprobe spectra obtained after diphenylsulfide and DBT reactions for Al_{13}–[$AlMo_6$] and [VMo_6] composites which

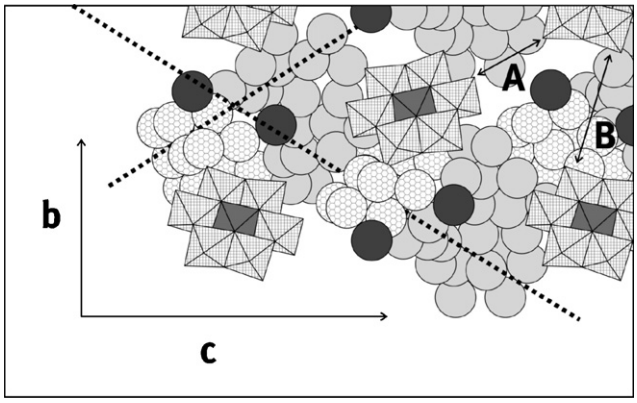

Fig. 14. Characteristic plane of the reticular system for Al_{13}–[$AlMo_6$] composite according to Ho Son et al. [37].

are the most active catalysts. In general, a good agreement was observed in the position of more intense lines that denoted the strength of bonds of the active site Mo = O_{2t}. However, the resolution of some lines was probably affected by the lower compound crystallinity and certain S adsorption during use.

According to these results, two of the most active composites were chosen to be re-used in the selective oxidation of diphenylsulfide. The conversion data are for Al_{13}–[$AlMo_6$], first use: 94%

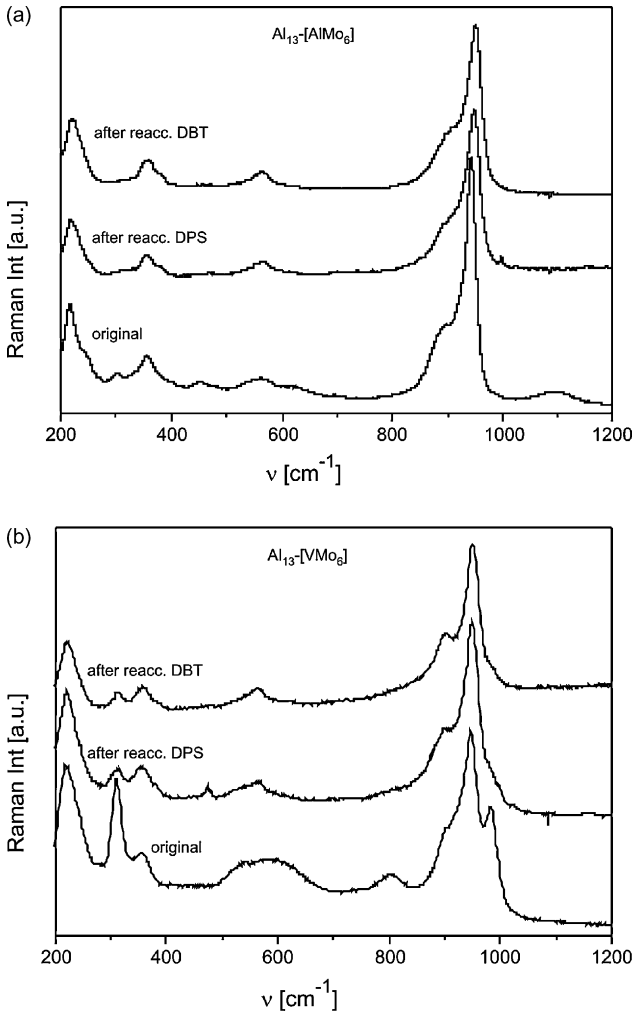

Fig. 15. Raman Microprobe spectra of (a) Al_{13}–[$AlMo_6$] and (b) Al_{13}–[VMo_6] composites before and after ODS reactions.

– second use: 45% and for Al_{13}–[$CrMo_6$], first use: 98% – second use: 80%. Results indicate that washing the material for making it recoverable is possible. These data have encouraged us to continue researching regeneration of catalyst composites.

4. Conclusions

New bi or trimetallic phases by reticular combination of Al_{13} isopolycation Keggin-type with different iso and heteropolymolybdates Anderson type as well as with two different polytungstate were obtained and characterized by several physico-chemical techniques. The proposed synthesis was an alternative method that enhances the reported technique to obtain Al_{13}–[$AlMo_6$].

^{27}Al MAS NMR and Raman Microprobe spectroscopies seemed to be the best techniques to reveal more clearly the structural preservation of heteropolyanions "anchored" in the Al_{13} matrix.

On the basis that structurally varied W and Mo–Al–O systems were interesting as catalysts for aromatic sulfide oxidation reactions, the prepared composites were proved in two clean typical oxidation processes: diphenylsulfide (DPS) to diphenylsulfone in presence of H_2O_2 and dibenzothiophene (DBT) to dibenzothiophenone by means of *tert-butyl* hydroperoxide (*t*-BuOOH). Both reactions were carried out in batch at 80 and 75 °C, respectively. The catalytic test for DPS oxidation led to yields and selectivity over 90% in sulfone by using composites based on Anderson derivatives species with Al and V. The activity can be associated to the presence of specific $AlMo_6$ entities and the differences between activity for the DPS–DBT oxidation is attributed to the lower S electron density in the last substrate. On the other hand, similar performance in DPS reaction was observed for the composite based on P-polytungstate. ^{27}Al MAS NMR and Raman spectroscopies proved to be very useful techniques for revealing the structural preservation, properties associated to the DPS reactivity and suggest interesting possibilities of re-use.

The advantages of this methodology are operational simplicity, recoverable and no corrosive catalyst, mild conditions, short reaction time and good yields. The use of solid catalyst allows replacement of the usual soluble inorganic acids, contributing to the waste reduction.

Acknowledgments

We are grateful to Mrs. Graciela Valle and Lic. Diego Peña for their contributions in experimental measurements. Authors would like to thank Bertrand Revel for his contribution for the NMR spectra acquisition and Dominique Massiot for fruitful discussions. Financial support from CONICET, CICPBA (Argentina) and MINCyT-ECOS Sud France Program is gratefully acknowledged. C.I. Cabello is a member of the research staff of CICPBA, Argentina.

References

[1] T. Kabe, A. Ishihara, W. Qian, in: Kodansha Scientific (Ed.), Hydrodesulfurization and Hydrodenitrogenation, Wiley-VCH, Tokyo, New York/Berlin, 1999.
[2] D.D. Whitehurst, T. Isoda, I. Mochida, Adv. Catal. 42 (1998) 345.
[3] D. Wang, E. Weihua Qian, H. Amano, K. Okata, A. Ishihara, T. Kabe, Appl. Catal. A: Gen. 253 (2003) 91.
[4] S. Patai, Z. Rappoport, The Synthesis of Sulphones, Sulphoxides, and Cyclic Sulphides, Wiley, New York, 1994.
[5] E. Clark, Kirk-Othmer, in: J.I. Kroschwitz, M. Howe-Grant (Eds.), Encyclopedia of Chemical Technology, 23, 4th ed., Wiley, New York, 1997, p. 134.
[6] R. Varma, R. Sain, H. Meshram, Tetrahedron Lett. 38 (1997) 6525 (and references cited therein).
[7] M. Tajbakhsh, R. Hosseinzadeh, A. Shakoori, Tetrahedron Lett. 45 (2004) 1889 (and references cited therein).
[8] D. Barton, W. Li, J. Smith, Tetrahedron Lett. 39 (1998) 7055.
[9] T. Iwahana, S. Sakaguchi, Y. Ishii, Tetrahedron Lett. 39 (1998) 9059.
[10] F. Bonadies, F. De Angelis, L. Locati, A. Scettri, Tetrahedron Lett. 37 (1996) 7129.
[11] S. Martin, L. Rossi, Tetrahedron Lett. 42 (41) (2001) 7147.
[12] A. Suarez, L. Rossi, S. Martin, Tetrahedron Lett. 36 (8) (1995) 1201.
[13] W. Xu, Y. Li, Q. Zhang, H. Zhu, Synthesis 2 (2004) 227.
[14] H. Gunaratne, M. McKervey, S. Feutren, J. Finlay, J. Boyd, Tetrahedron Lett. 39 (1998) 5655.
[15] M. Matteucci, G. Bhalay, M. Bradley, Org. Lett. 5 (3) (2003) 235.
[16] M. Palucki, P. Hanson, E. Jacobsen, Tetrahedron Lett. 33 (47) (1992).
[17] B. Saito, T. Katsuki, Tetrahedron Lett. 42 (23) (2001).
[18] K.S. Kim, H. Hwang, Ch. Cheong, C. Hahn, Tetrahedron Lett. 31 (20) (1990).
[19] S. Oae, Y. Watanabe, K. Fujimori, Tetrahedron Lett. 24 (52) (1983) 5903.
[20] J.E. Barker, T. Ren, Tetrahedron Lett. 46 (40) (2005) 6805.
[21] M. Lakshmi Kantam, B. Neelima, Ch. Venkat Reddy, M.K. Chaudhuri, S.K. Dehury, Catal. Lett. 95 (1–2) (2004) 19.
[22] S. Otsuki, T. Nonaka, W. Qian, A. Ishihara, T. Kabe, Sekiyu Gakkaishi 44 (2001).
[23] T. Aida, Shokubai 37 (1995) 243.
[24] T. Aida, D. Yamamoto, Prep. Am. Chem. Soc. Div. Fuel Chem. 39 (1994) 623.
[25] F.M. Collins, A.R. Lucy, C. Sharp, J. Mol. Catal. A: Chem. 117 (1997) 397.
[26] S.E. Bonde, W. Gore, G.E. Dolbear, E.R. Skov, Prep. Am. Chem. Soc. Div. Pet. Chem. 45 (2) (2000) 364.
[27] S.E. Bonde, W. Gore, G.E. Dolbear, Prep. Am. Chem. Soc., Div. Pet. Chem. 44 (2) (1999) 199.
[28] G.E. Dolbear, E.R. Skov, Prep. Pap. Am. Chem. Soc. Div. Pet. Chem. 45 (2) (2000) 375.
[29] S. Otsuki, T. Nonaka, W. Qian, A. Ishihara, T. Kabe, Sekiyu Gakkaishi 42 (1999) 315.
[30] M. Te, C. Fairbridge, Z. Ring, Appl. Catal. 219 (2001) 267.
[31] C.I. Cabello, I.L. Botto, H.J. Thomas, Appl. Catal. A 197 (2000) 79.
[32] C. Lamonier, C. Martin, J. Mazurelle, V. Harlé, D. Guillaume, E. Payen, Appl. Catal. B: Environ. 70 (1–4) (2007) 548.
[33] C. Venturello, R. D'Aloisio, J.C.J. Bart, M. Ricci, J. Mol. Catal. 32 (1985) 107.
[34] F.P. Ballistreri, G.A. Tomasselli, R.M. Toscano, V. Conte, F.D. Furia, J. Mol. Catal. 89 (1994) 295.
[35] L. Salles, C. Aubry, R. Thouvenot, F. Robert, C. Doremieux-Morin, G. Chottard, H. Ledon, Y. Jeannin, J. Bregeault, Inorg. Chem. 33 (1994) 871.
[36] L. Salles, C. Aubry, F. Robert, G. Chottard, R. Thouvenot, H. Ledon, J. Bregeault, New J. Chem. 17 (1993) 367.
[37] J. Ho Son, H. Choi, Y. Uk Kwon, J. Am. Chem. Soc. 122 (2000) 7.
[38] M. Muñoz, C.I. Cabello, I.L. Botto, G. Minelli, M. Capron, C. Lamonier, E. Payen, J. Mol. Struct. 831 (2007) 96.
[39] C.I Cabello, I.L. Botto, J. Filace, G. Minelli, M. Occhiuzzi, D. Cordischi, J. Porous Mater. 14 (3) (2007) 331.
[40] C. Martin, C. Lamonier, M. Fournier, D. Mentré, D. Guillaume, V. Harlé, E. Payen, Chem. Mater. 17 (2005) 4438.
[41] C.I. Cabello, F.M. Cabrerizo, A. Alvarez, H.J. Thomas, J. Mol. Catal. A: Chem. 186 (2002) 89.
[42] J. Ho Son, Y. Uk Kwon, O. Hee Han, Inorg. Chem. 42 (2003) 4153.
[43] J. Ho Son, Y. Uk, Kwon, Inorg. Chem. 43 (2004) 1929.
[44] C.I. Cabello, M.G. Egusquiza, I.L. Botto, G. Minelli, Mater. Chem. Phys. 87 (2004) 264.
[45] A. Samoson, E. Lippmaa, Phys. Rev. B 28 (1983) 6567.
[46] L. Frydman, J.S. Harwood, J. Am. Chem. Soc. 117 (1995) 5367.
[47] J.P. Amoureux, C. Fernandez, S. Steuernagel, J. Magn. Reson. 123 (1) (1996) 116.
[48] J.P. Amoureux, C. Fernandez, Solid State Nucl. Magn. Reson. 10 (1998) 281.
[49] W.H. Casey, Chem. Rev. 106 (1) (2006) 1.
[50] L. Allouche, C. Huguenard, F. Phys. Chem. Sol. 62 (2001) 1525.
[51] D. Massiot, F. Fayon, M. Capron, I. King, S. Le Calvet, B. Alonso, J.-O. Durand, B. Bujoli, Z. Gan, G. Hoatson, Magn. Reson. Chem. 40 (2002) 70.
[52] J.-B. d'Espinose de Lacaillerie, C. Fretigny, D. Massiot, J. Magn. Reson. 192 (2008) 244.
[53] I.L. Botto, A.C. Garcia, H.J. Thomas, J. Chem. Sol. 53 (8) (1992) 1075.
[54] A. Björnberg, Acta Crystallogr. B35 (1979) 1995.
[55] F.D. Hardcastle, I.E. Wachs, J. Phys. Chem. 95 (1991) 5031.
[56] L. Salles, J.Y. Piquemal, R. Thouvenot, C. Minot, J.-M. Brégeault, J. Mol. Catal. A 117 (1997) 375.
[57] S. Otsuki, T. Nonaka, N. Takashima, W. Quian, A. Ishihara, T. Imai, T. Kabe, Energy Fuels 14 (2000) 1232.